Solid-State Near-Infrared Circularly Polarized Luminescence from Chiral YbIII-Single-Molecule Magnet

Bertrand Lefeuvre, Carlo Andrea Mattei, Jessica Flores Gonzalez, Frédéric Gendron, Vincent Dorcet, François Riobé, Claudia Lalli, Boris Le Guennic, Olivier Cador, Olivier Maury, et al.

10.1002/chem.202100903

WILEY-VCH

COMMUNICATION

Solid-State Near-Infrared Circularly Polarized Luminescence from Chiral Yb^{III}-Single-Molecule Magnet

Bertrand Lefeuvre,[a] Carlo Andrea Mattei,[a] Jessica Flores Gonzalez,[a] Frédéric Gendron,[a] Vincent Dorcet,[a] François Riobé,[b] Claudia Lalli,[a] Boris Le Guennic,*[a] Olivier Cador,[a] Olivier Maury,[b] Stéphan Guy,[c] Amina Bensalah-Ledoux,[c] Bruno Baguenard,*[c] Fabrice Pointillart,*[a]

[a] B. Lefeuvre, C. A. Mattei, Dr. J. Flores Gonzalez, Dr. F. Gendron, Dr. V. Dorcet, Dr. C. Lalli, Dr. B. Le Guennic, Prof. O. Cador, Dr. F. Pointillart
Univ Rennes, CNRS, ISCR (Institut des Sciences Chimiques de Rennes) - UMR 6226, 35000 Rennes, France
E-mail: fabrice.pointillart@univ-rennes1.fr
[b] Dr. F. Riobé, Dr. O. Maury
Univ Lyon, Ens de Lyon, CNRS UMR 5182, Université Claude Bernard Lyon 1, Laboratoire de Chimie, F69342, Lyon, France
[c] Prof. S. Guy, Dr. A. Bensalah-Ledoux, Dr. B. Baguenard
Univ Lyon, Université Claude Bernard Lyon 1, CNRS, UMR 5306, Institut Lumière Matière, F-69622 Lyon, France.

Supporting information for this article is given via a link at the end of the document.

Abstract: A field-induced chiral Yb^{III} Single-Molecule Magnet (SMM) displayed an unprecedented near-infrared circularly polarized luminescence (NIR-CPL) in solid-state. The bridging bis(1,10-phenantro[5,6b])tetrathiafulvalene triad (**L**) allowed an efficient sensitization of the NIR $^2F_{5/2} \rightarrow {}^2F_{7/2}$ emission while the NIR-CPL is associated to the *f-f* transitions of the Yb^{III} ion bearing chiral β-diketonate derived-camphorate ancillary ligands.

Circularly Polarized Luminescence (CPL) is defined as the difference of intensity between the spontaneous emission of left circularly vs. right-circularly polarized light by chiral molecular systems.[1] To date, CPL has been used mainly to investigate configurational and conformational changes in chemical and biological edifices in bio-assays[1b],[2] because it combines the sensitivity of luminescence measurements with a high responsiveness to chiral environment.[3] Moreover, applications in chiral electronics (*e.g.* circularly polarized OLEDs) are of interest for CPL-emitting materials as well as for storage devices.[4] A convenient way to express the CPL activity is the dissymmetry factor $g_{lum} = 2(I_L–I_R)/(I_L+I_R)$, where I_L and I_R stand for the intensity of the left- and right circularly polarized emissions, respectively. Whereas the g_{lum} values for chiral organic molecules are often lower than 0.01,[5] chiral lanthanide complexes can exhibit much higher values. Usually, enantiopure Eu^{III} and Tb^{III} complexes – the most emissive Ln^{III} ions – present transitions with g_{lum} values between 0.1 and 1.4. The largest g_{lum} values were obtained for trivalent lanthanide associated to β-diketonate derived camphorato anions.[6] Among them, the highest value of g_{lum} = 1.38 measured for the $Cs[Eu((+)\text{-hfbc})_4]$ complex (where hfbc = 3-heptafluoro-butylryl-(+)-camphorato).[7] Another chemical approach is to associate achiral $Ln(\beta\text{-diketonate})_n$ ($2 \leq n \leq 4$) units to chiral ligands such as binaphtyl derivatives,[8] cyclohexane diamine,[9] or pyridinebisoxazoline.[10] In the near infrared (NIR) region i.e. from 700 to 1300 nm, Nd^{III} and mostly Yb^{III}-centered emissions are likely to be favoured, even if NIR-CPL studies for these ions remain scarce.[10][11]

High g_{lum} values for lanthanide complexes originate from intraconfigurational Laporte-forbidden *f-f* transitions obeying magnetic dipole selection rules. Owing to weak *f-f* absorption bands, lanthanide excited-states cannot be efficiently populated by a direct process. However, the sensitization can be efficiently achieved by an indirect energy/electron transfer from an organic ligand that acts as an antenna. In this respect, some of us successfully sensitized NIR emitters such as Yb^{III} ions by using push-pull ligands with strong absorption coefficients in the visible region.[12] In that sense, tetrathiafulvalene (TTF)-based ligands are particularly suitable for the sensitisation of NIR emitters such as Nd^{III},[13] Yb^{III}[14] and Er^{III}[15].

Besides these spectroscopic properties, *f*-block elements play a major role in the development of molecular magnetic materials known as Single-Molecule Magnets (SMMs).[16] These species exhibit a magnetic memory effect at the molecular scale at a temperature up to 80 K[17] and thus present potential applications in data storage and/or quantum computing.[18] Importantly, based on an idea initially proposed by van Vleck in 1937,[19] the crystal-(ligand)-field splitting (CFS) of the ground multiplet for a mononuclear lanthanide complex is at the origin of both the luminescence fine structure and thermal variation of the magnetic susceptibility. In this context, we and others proposed to use the lanthanide luminescence spectroscopy as a tool to probe the energy splitting of the ground multiplet and fully rationalize molecular magnetism results.[20]

In the present contribution, we report a Yb-based near infrared circularly polarized luminescent single-molecule magnet (NIR-CPL SMM) taking advantage of i) the 3-trifluoro-acetyl-(+)-camphorato (facam) ancillary ligand to promote large g_{lum} values, ii) the bis(1,10-phenantro[5,6b])tetrathiafulvalene triad (**L**)[21] as efficient organic chromophore and iii) the Yb^{III} ion as NIR emitter and source of magnetic anisotropy for the observation of SMM behavior.[22] To the best of our knowledge, there are only two examples of lanthanide compounds showing both visible range CPL and SMM behaviour.[23] Thus, the two enantiomers of $[Yb(facam)_3(\mathbf{L})]_2$ (**(+)Yb** and **(-)Yb**) were prepared and their structural, magnetic, optical and chiroptical properties were experimentally and theoretically studied.

Both **(+)Yb** and **(-)Yb** are isostructural (Table S1) and the structural description is given for **(-)Yb**. It crystallizes in the chiral C2 (N°5) monoclinic space group (Table S1). The two terminal Yb^{III} ions are linked to three $facam^-$ chiral ancillary ligands and one 1,10-phenanthroline (phen) extremity of the **L** ligand conferring a

10.1002/chem.202100903

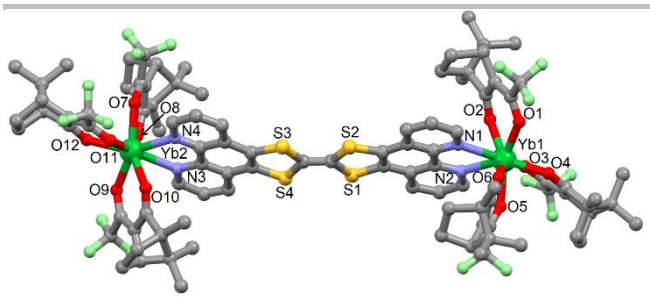

Figure 1. Molecular structure of the dinuclear complex **(-)Yb**. Carbon (grey), fluorine (green), oxygen (red), nitrogen (blue), sulphur (yellow) and ytterbium (dark green).

N_2O_6 first coordination polyhedron with a very similar D_{4d} symmetry for both Yb^{III} ions (Table S2, Figures 1 and S1). The distortion is visualized by continuous shape measures performed with SHAPE 2.1 (square antiprism, $CShM_{SAPR-8}$ = 0.567 and 0.554 for Yb1 and Yb2, respectively. Table S2).[24] **L** plays the role of redox bridging ligand (vide infra) between the two terminal [Yb(-)(facam)$_3$] thanks to the double coordination of the phen moieties. The central C=C bond length (1.335(13) Å) agrees with the neutral form of the bridging ligand. The crystal packing did not show any significant π-π stacking or S···S short contact (Figure S2) contrary to what observed in the X-ray structure of the achiral Dy^{III} analogue [Dy(hfac)$_3$**L**]$_2$·CH_2Cl_2·C_6H_{14} (where hfac$^-$ = 1,1,1,5,5,5-hexafluoroacetylacetonate).[21b] The higher steric hindrance of the facam$^-$ anions compared to hfac$^-$ could explain this difference. Nevertheless the coherence of the crystal packing for **(-)Yb** was guaranteed thanks to short S2···O3 (3.175 Å) contacts between the TTF core and one facam$^-$ ligand of the neighbouring molecule. The reversible redox-activity of the two enantiomers was demonstrated by cyclic voltammetry in CH_2Cl_2 solution and present the expected characteristic of TTF-containing lanthanide complexes[21] (Figure S3 and see SI for more details).

The room temperature value of the $\chi_M T$ product for **(+)Yb** (where χ_M is the molar magnetic susceptibility) is 4.73 cm^3 K mol^{-1} which is in agreement with two Yb^{III} free ions (expected value of 5.14 cm^3 K mol^{-1}) (Figure S4).[25] The depopulation of the M_J doublet states led to a monotonic decrease of $\chi_M T$ down to 3.03 cm^3 K mol^{-1} at 2 K. At such temperature the field dependence of the magnetization showed a classical behavior with a value of 3.48 Nβ at 50 kOe (see Figure S4). Because the binuclear system is almost centro-symmetric, SA-CASSCF/RASSI-SO calculations were performed on one half of the system starting from the X-ray structure of **(-)Yb** while dynamical correlation effects were taken into account by means of subsequent CASPT2 calculations (see Computational Details), as usual for Yb^{III} complexes.[26] The energy splitting calculated for the $^2F_{7/2}$ multiplet state allowed a correct reproducibility of both thermal variation of the $\chi_M T$ product and magnetization at 2 K (Figure S4). Indeed, the agreement between experimental data and computational results could be considered satisfying with respect to the difficulty in quantitatively reproducing the experimental magnetic properties of Yb^{III} complexes.[26][27] The ground state is composed of an admixture of |7/2, ±M_J > states (60% |±7/2>, 16% |±5/2> and 14% |±3/2>) giving the following g-factors: g_x = 0.86, g_y = 1.38 and g_z = 6.19 (Table S4). The main anisotropy axis is localized in the plane formed by the two coordinated nitrogen atoms as expected for prolate ions in N_2O_6 environment (Figure S5).[26] No frequency dependence of χ_M'' for **(+)Yb** was observed in zero external direct-current (dc) field (Figure S6) due to the possible fast relaxation through Quantum Tunnelling of the Magnetization (QTM) as observed for Yb^{III} coordination complexes[22] and confirmed by the calculated non-zero transversal contributions of the g-factors (see Figure S12 and Table S4). In order to suppress the QTM, the optimal dc field of 1200 Oe was determined by field dependence of the relaxation time (Figure S6). In such an applied field, both in-phase (Figure S7) and out-of-phase (Figure 2) components of the magnetic susceptibility were observed. Both field (Table S5) and temperature (Table S6) variations of the magnetic susceptibility can be analysed in the framework of an extended Debye model (Figure S8). The applied 1200 Oe magnetic field and the field dependence of the relaxation times strongly supports the absence of both QTM and direct relaxation processes. The Arrhenius plot of the relaxation time could be well fitted by a combination of Orbach and Raman mechanisms: $\tau^{-1} = \tau_0^{-1}\exp(-\Delta/kT) + CT^n$ with τ_0 = 4.02(28)×10^{-7} s, Δ = 21.7(6) K, C = 107.7(210) s $K^{-2.94}$ and n = 2.94(28) (Figure 2). The expected value for n ranges between 4 and 9 depending of the ground state doublets energies for Kramers ions.[28] Nevertheless, the presence of both acoustic and optic phonons in specific ligand environments such as N_2O_6[29] can lead to a value close to 2.[30]

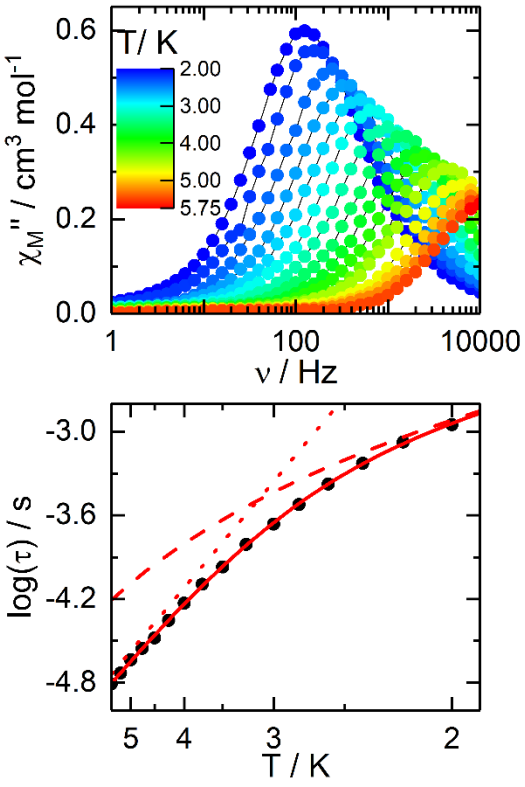

Figure 2. (Top) Frequency dependence of the out-of phase component of the magnetic susceptibility under an applied magnetic field of 1200 Oe between 2 and 5.75 K for **(+)Yb**. (Bottom) Arrhenius plots of the temperature dependence of the relaxation time in a 1200 Oe applied magnetic field (full black disks) with the best-fitted curve (red line) and the two decomposed Orbach (dotted red line) and Raman (dashed red line) relaxation processes in the temperature range 2-5.25 K.

10.1002/chem.202100903

The Orbach magnetic relaxation process is only a minor contribution since the energy barrier (21.7 K) determined from the magnetic measurements is much weaker than the energy gap between the two highest energy emission contributions (464 K) and calculated KD0-KD1 splitting (394 K, vide infra). Figure S9 depicts the Cole-Cole plots[31] normalized to their isothermal values. Such representation highlights that almost 100 % of the sample slowly relaxed under an applied 1200 Oe magnetic field through an almost single relaxation time since α ranges from 0.05 to 0.14 between 5.5 and 2 K (Table S6).

UV-visible absorption and Electronic Circular Dichroism (ECD) of both enantiomers have been studied in CH_2Cl_2 solution (Figure S10). The experimental absorption curves for both **(+)Yb** and **(-)Yb** enantiomers are superimposed. Based on previous published papers,[6a][20a] the lowest energy contribution was attributed to the HOMO→LUMO Intra-Ligand Charge Transfer (ILCT) of **L** while the following contributions come from π-π* intra-facam$^-$ and intra-phen excitations. Emission properties of **(+)Yb** and **(-)Yb** were first measured in CH_2Cl_2 solution at room temperature (Figure S11). Upon irradiation at 300 nm (33000 cm^{-1}) a NIR emission centred at 10000 cm^{-1} is detected that corresponds to the $^2F_{5/2} \rightarrow {}^2F_{7/2}$ transition. No significant residual ligand-centred emission is observed, indicating an efficient sensitization process through antenna effect as already observed for other TTF-centred chromophores.[20a] The room temperature emission spectra are composed of three main components localized at 10194, 9872 and 9671 cm^{-1} and one shoulder at higher energy. NIR emission of the Yb^{III} was also detected in solid-state at room temperature and 10 K (Figure 3). The low temperature measurements allowed (i) to assign the high energy contribution (10500 cm^{-1}) observed at room temperature to a hot band coming from the M_j excited state of the $^2F_{5/2}$ multiplet and (ii) to identify three emitting contributions, over the 4 expected for such symmetry signature, for the $^2F_{7/2}$ CFS at 10204, 9901 and 9653 cm^{-1}. The total splitting of 551 cm^{-1} falls down in the expected splitting value for Yb^{III} complex in low symmetry.[26b,c] The calculated crystal-field splitting is in agreement with the total splitting given by the luminescence at 10 K and also reveals that the broad character of the second band is due to the contribution of two transitions (Figure 3).

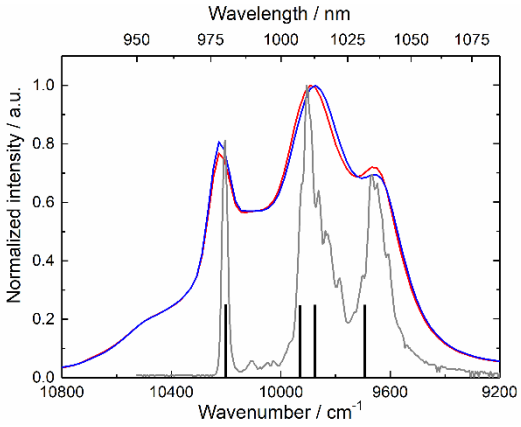

Figure 3. NIR luminescence spectra in solid-state under an irradiation of 360 nm (27778 cm^{-1}) for both enantiomers **(+)Yb** (in red) and **(-)Yb** (in blue) at room temperature and under an irradiation of 450 nm (22222 cm^{-1}) for **(+)Yb** (in gray) at 10 K. Vertical black sticks represent the computed relative energy splitting.

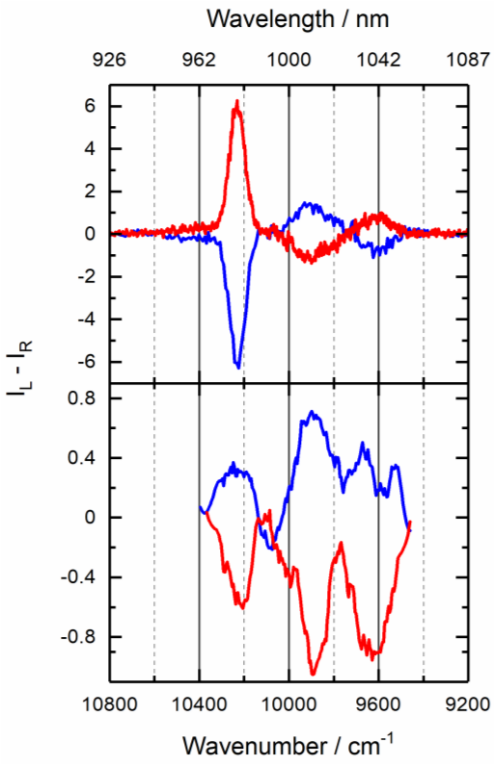

Figure 4. (top) NIR CPL spectra of both enantiomers **(+)Yb** (in red) and **(-)Yb** (in blue) in CH_2Cl_2 solution at room temperature (C = 5×10^{-5} M) under a 300 nm (33300 cm^{-1}) irradiation. (bottom) NIR CPL spectra of both enantiomers **(+)Yb** (in red) and **(-)Yb** (in blue) in solid-state at room temperature under a 360 nm (27778 cm^{-1}) irradiation. The CPL signal is given after rescaling: normalization with respect to maximum of emission at 1013 nm and magnification by a 10^3 factor for convenient lecture.

Thus, the calculated splitting of the $^2F_{7/2}$ multiplet (0, 274, 319 and 501 cm^{-1} at the CAS(13,7)PT2-SO level, Table S4) fits well the experimental emission lines. From solution (Figure S12) to solid state (Figure 3), the NIR fluorescence spectra of Yb^{III} present the same energy transitions but different relative intensities. The most intense band is the one at the highest energy for the solution, while it is the central one for the solid state. The intensity ratio between these two bands decreases by a factor 2 from solution to solid state. Finally, the luminescence lifetime has been measured for **(+)Yb** in the solid state (Figure S13) and fitted with a mono-exponential decay giving τ = 12,6 µs. This value is similar to related complexes already reported in the literature.[26b] CH_2Cl_2 solution-state ECD measurements, performed at room temperature, for **(+)Yb** and **(-)Yb** confirmed their enantiomeric nature (Figures S10 and S14). Cotton effect is composed of three dichroic contributions of opposite signs localized at the same energies than the absorption bands attributed to the facam$^-$ ancillary anions i.e. 30300 cm^{-1}, 32900 cm^{-1} and 40000 cm^{-1}. The absence of the lowest energy transition centered on the TTF ligand suggests that the ECD spectra are dominated by contributions coming from the facam$^-$ ligands. NIR-CPL was investigated in CH_2Cl_2 solution at room temperature for the two enantiomers. Three main bands could be identified as positive (10235 cm^{-1}), negative (9891 cm^{-1}) and positive (9625 cm^{-1}) contributions for **(+)Yb** (Figure 4). A mirror image was obtained

for the **(-)Yb** enantiomer. The room temperature dissymmetry g_{lum} factor[11b] can be determined for each CPL contribution with the values of +/-0.013 for the sharp intense band around 10235 cm^{-1}, -/+0.004 for the band around 9891 cm^{-1} and +/-0.002 for the band around 9625 cm^{-1} for **(+)/(-)-Yb**, respectively. These values are in the same range as those previously reported in the literature.[10] Finally, NIR-CPL in solid-state was measured at room temperature under an irradiation of 360 nm (27778 cm^{-1}) giving rise to three contributions (Figures 4 and S15). Importantly, the position of the CPL bands is not affected by the change of state. However, CPL measurements in solid state were much more difficult to record. Indeed, solid state's CPL signals are dramatically reduced and a numerical Savitsky-Golay filter (3rd order, 10 neighbours) is thus required to plot the spectra. For instance, the band splitting at 9600 cm^{-1} is a noise artefact. In addition to the CPL signal drop from solution to solid state, the overall shape of the CPL spectra is profoundly changed in term of relative intensities of the three transitions as well as their sign. These spectral change between two states, also observed in fluorescence (branching ratio changes, see above) are much more pronounced in the CPL spectra. For instance, the most intense transition in solution (10235cm^{-1}, $|g_{lum}|$=0.013), displays a sign inversion in solid state and its intensity drops down to $|g_{lum}|$=0.001. These spectral changes reveal a modification of the rare earth surrounding between the two states, mainly due to the reorganisation of the facam$^-$ ancillary ligands, and/or a reduction of conformers population in the solid state.

In conclusion, the two enantiomers of a chiral Yb^{III} dinuclear complex were obtained by bridging two $Yb(facam)_3$ units by the bis(1,10-phenantro[5,6b])tetrathiafulvalene triad (**L**). Thanks to the juxtaposition of judicious ingredients such as (i) chiral facam$^-$ ancillary ligands, (ii) excellent photosensitizing bridging ligand **L** acting as a light harvesting antenna to efficiently sensitize the NIR luminescence of Yb^{III} ion, (iii) strong magnetic anisotropy of the Yb^{III} ion, an unprecedented combination of field-induced Single-Molecule Magnet behavior and NIR Circularly Polarized Luminescence was observed in solid-state for the dinuclear complex $[Yb(facam)_3(\mathbf{L})]_2$. The first observation of Yb^{III} NIR-CPL in solid-state allowed to show drastic modification of such signal changing from CH_2Cl_2 solution to solid-state. This redox-active chiral NIR circularly polarized luminescent field-induced single-molecule magnet paves the route to the modulation of both chiroptical and magnetic properties through the oxidation state of the bridging TTF-based triad.

Acknowledgements

This work was supported by the CNRS through the PRC MULTISWITCH (N°227606), Université de Rennes 1, the European Commission through the ERC-CoG 725184 MULTIPROSMM (project n. 725184) and the Agence Nationale de la Recherche (SMMCPL ANR-19-CE29-0012-02). B.L.G. and F.G. thank the French GENCI/IDRIS-CINES centre for high-performance computing resources and Région Bretagne for SAD Grant (SAD18006-LnCPLSMM). Y. Guyot from ILM is thanked for the NIR luminescence lifetime measurements.

Keywords: ytterbium • triad • chiral ancillary ligand • circularly polarized luminescence • single molecule magnet

[1] a) J. P. Riehl, F. S. Richardson, *Chem. Rev.* **1986**, *86*, 1-16; b) R. Carr, N. H. Evans, D. Parker, *Chem. Soc. Rev.* **2012**, *41*, 7673-7686.

[2] F. Zinna, L. Di Bari, *Chirality* **2015**, *27*, 1-13.

[3] a) J. Yuasa, T. Ohno, H. Tsumatori, R. Shiba, H. Kamikubo, M. Kataoka, Y. Hasegawa, T. Kawai, *Chem. Commun.* **2013**, *49*, 4604-4606; b) M. Leonzio, A. Melchior, G. Faura, M. Tolazzi, M. Bettinelli, F. Zinna, L. Arrico, L. Di Bari, F. Piccinelli, *New J. Chem.* **2018**, *42*, 7931-7939.

[4] a) J. R. Brandt, F. Salerno, M. J. Fuchter, *Nat. Rev. Chem.* **2017**, *1*, 0045; b) F. Zinna, M. Pasini, F. Galeotti, C. Botta, L. Di Bari, U. Giovanella, *Adv. Funct. Mater.* **2017**, *27*, 1603719; c) J. Han, S. Guo, H. Lu, S. Liu, Q. Zhao, W. Huang, *Adv. Opt. Mater.* **2018**, 1800538.

[5] a) P. M. Burrezo, V. G. Jiménez, D. Blasi, I. Ratera, A. G. Campana, J. Veciana, *Angew. Chem. Int. Ed.* **2019**, *58*, 16282-16288; b) H. Isla, N. Saleh, J.-K. Ou-Yang, K. Dhbaibi, M. Jean, M. Dziurka, L. Favereau, N. Vanthuyne, L. Toupet, B. Jamoussi, M. Srebo-Hooper, J. Crassous, *J. Org. Chem.* **2019**, *84*, 5383-5393; c) L. Guy, M. Mosser, D. Pitrat, J.-C. Mulatier, M. Kukulka, M. Srebo-Hooper, E. Jeanneau, A. Bensalah-Ledoux, B. Baguenard, S. Guy, *J. Org. Chem.* **2019**, *84*, 10870-10876.

[6] a) T. Harada, Y. Nakano, M. Fujiki, M. Naita, T. Kawai, Y. Hasegawa, *Inorg. Chem.* **2009**, *48*, 11242-11250; b) J. Yuasa, H. Ueno, T. Kawai, *Chem. Eur. J.* **2014**, *20*, 8621-8627.

[7] J. L. Lunkley, D. Shirotani, K. Yamanari, S. Kaizaki, G. Muller, *J. Am. Chem. Soc.* **2008**, *130*, 13814-13815.

[8] a) N. Koiso, Y. Kitagawa, T. Nakanishi, K. Fushimi, Y. Hasegawa, *Inorg. Chem.* **2017**, *56*, 5741-5747; b) D. Liu, Y. Zhou, Y. Zhang, H. Li, P. Chen, W. Sun, T. Gao, P. Yan, *Inorg. Chem.* **2018**, *57*, 8332-8337; d) A. J. Jalilah, F. Asanoma, M. Fujiki, *Inorg. Chem. Front.* **2018**, *5*, 2718-2733.

[9] M. Leonzio, M. Bettinelli, L. Arrico, M. Monari, L. Di Bari, F. Piccinelli, *Inorg. Chem.* **2018**, *57*, 10257-10264.

[10] F. Zinna, L. Arrico, L. Di Bari, *Chem. Commun.* **2019**, *55*, 6607-6609.

[11] a) C. L. Maupin, D. Parker, J. A. Gareth Williams, J. P. Riehl, *J. Am. Chem. Soc.* **1998**, *120*, 10563-10564; b) F. Gendron, S. Di Pietro, L. Abad Galan, F. Riobé, V. Placide, L. Guy, F. Zinna, L. Di Bari, A. Bensalah-Ledoux, Y. Guyoy, G. Pilet, F. Pointillart, B. Baguenard, S. Guy, O. Cador, O. Maury, B. Le Guennic, *Inorg. Chem. Front.* **2021**, *8*, 914-926.

[12] A. D'Aléo, F. Pointillart, L. Ouahab, C. Andraud, O. Maury, *Coord. Chem. Rev.* **2012**, *256*, 1604-1620.

[13] F. Pointillart, B. Le Guennic, O. Maury, S. Golhen, O. Cador, L. Ouahab, *Inorg. Chem.* **2013**, *52*, 1398-1408.

[14] F. Pointillart, T. Cauchy, O. Maury, Y. Le Gal, S. Golhen, O. Cador, L. Ouahab, *Chem. Eur. J.* **2010**, *16*, 11926-11941.

[15] F. Pointillart, A. Bourdolle, T. Cauchy, O. Maury, Y. Le Gal, S. Golhen, O. Cador, L. Ouahab, *Inorg. Chem.* **2012**, *51*, 978-984.

[16] D. N. Woodruff, R. E. P. Winpenny, R. A. Layfield, *Chem. Rev.* **2013**, *113*, 5110-5148.

[17] a) C. A. P. Goodwin, F. Ortu, D. Reta, N. F. Chilton, D. P. Mills, *Nature* **2017**, *548*, 439-442; b) F.-S. Guo, B. M. Day, Y.-C Chen, M.-L. Tong, A. Mansikkamäki, R. A. Layfield, *Science* **2018**, *362*, 1400-1403.

[18] a) G. Aromi, D. Aguila, P. Gamez, F. Luis, O. Roubeau, *Chem. Soc. Rev.* **2012**, *41*, 537-546; b) S. Thiele, F. Balestro, R. Ballou, S. Klyatskaya, M. Ruben, W. Wernsdorfer, *Science* **2014**, *344*, 1135-1138.

[19] J.-H. Van Vleck, *J. Phys. Chem.* **1937**, *41*, 67-80.

[20] a) F. Pointillart, B. Le Guennic, O. Cador, O. Maury, L. Ouahab, *Acc. Chem. Res.* **2015**, *48*, 2834-2842; b) J. Long, Y. Guari, R. A. S. Ferreira, L. D. Carlos, J. Larionova, *Coord. Chem. Rev.* **2018**, *363*, 57-70; c) R. Marin, G. Brunet, M. Murugesu, *Angew. Chem. Int. Ed.* **2021**, *60*, 1728-1746; d) D. Guettas, F. Gendron, G. Fernandez Garcia, F. Riobé, T. Roisnel, O. Maury, G. Pilet, O. Cador and B. Le Guennic, *Chem. Eur. J.* **2020**, 26, 4389-4395.

[21] a) B. Chen, Z.-P. Lv, C. Hua, C. F. Leong, F. Tuna, D. M. D'Alessandro, D. Collison, J.-L. Zuo, *Inorg. Chem.* **2016**, *55*, 4606-4615; b) B. Lefeuvre, O. Galangau, J. Flores Gonzalez, V. Montigaud, V. Dorcet, L. Ouahab, B. Le Guennic, O. Cador, F. Pointillart, Front. *Chem.* **2018**, *6*, 552-570.

[22] F. Pointillart, O. Cador, B. Le Guennic, L. Ouahab, *Coord. Chem. Rev.* **2017**, *346*, 150-175.

[23] a) B. El Rez, J. Liu, V. Béreau, C. Duhayon, Y. Horino, T. Suzuki, L. Coolen, J.-P. Sutter, *Inorg. Chem. Front.* **2020**, *7*, 4527-4534; b) U. Huizi-Rayo, A. Zabala-Lekuona, A. Terenzi, C. M. Cruz, J. M. Cuerva, A.

Rodriguez-Diéguez, J. A. Garcia, J. M. Seco, E. San Sebastian, J. Cepeda, *J. Mater. Chem. C.* **2020**, *8*, 8243-8256.

[24] M. Llunell, D. Casanova, J. Cirera, J. M. Bofill, P. Alemany, S. Alvarez, SHAPE (version 2.1), Barcelona, **2013**.

[25] O. Kahn, Molecular Magnetism; VCH: Weinhem, **1993**.

[26] a) J. Jung, T. T. da Cunha, B. Le Guennic, F. Pointillart, C. L. M. Pereira, J. Luzon, S. Golhen, O. Cador, O. Maury, L. Ouahab, *Eur. J. Inorg. Chem.* **2014**, 3888−3894; b) F. Pointillart, J. Jung, R. Berraud-Pache, B. Le Guennic, V. Dorcet, S. Golhen, O. Cador, O. Maury, Y. Guyot, S. Decurtins, S.-X. Liu, L. Ouahab, *Inorg. Chem.* **2015**, *54*, 5384-5397.

[27] a) J.-L. Liu, K. Yuan, J.-D. Leng, L. Ungur, W. Wernsdorfer, F.-S. Guo, L. F. Chibotaru, M.-L. Tong, *Inorg. Chem.* **2012**, *51*, 8538−8544; b) P.-H. Lin, W.-S. Sun, Y.-M. Tian, P.-F. Yan, L. Ungur, L. F. Chibotaru, M. Murugesu, *Dalton Trans.* **2012**, *41*, 12349−12352; c) N. A. G. Bandeira, C. Daniel, A. Trifonov, M. J. Calhorda, *Organometallics* **2012**, *31*, 4693−4700.

[28] a) C. Dekker, A. F. M. Arts, H. W. de Wijn, A. J. van Duyneveldt, J. A. Mydosh, *Phys. Rev. B: Condens. Matter Mater. Phys.* **1989**, *40*, 11243−11251; b) J. Tang, P. Zhang, Lanthanide Single Molecule Magnets; Springer-Verlag: Berlin, **2015**.

[29] F. Pointillart, J.-K. Ou-Yang, G. Fernandez Garcia, V. Montigaud, J. Flores Gonzalez, R. Marchal, L. Favereau, F. Totti, J. Crassous, O. Cador, L. Ouahab, B. Le Guennic, *Inorg. Chem.* **2019**, *58*, 52-56.

[30] C. A. P. Goodwin, D. Reta, F. Ortu, N. F. Chilton, D. P. Mills, *J. Am. Chem. Soc.* **2017**, *139*, 18714−18724.

[31] K. S. Cole, R. H. Cole, *J. Chem. Phys.* **1941**, *9*, 341−351.

[32] a) Y. Kishi, L. Cornet, F. Pointillart, F. Riobé, B. Lefeuvre, O. Cador, B. Le Guennic, O. Maury, H. Fujiwara, L. Ouahab *Eur. J. Inorg. Chem.* **2018**, 458-468; b) S. Speed, M. Feng, G. Fernandez Garcia, F. Pointillart, B. Lefeuvre, F. Riobé, S. Golhen, B. Le Guennic, F. Totti, Y. Guyot, O. Cador, O. Maury, L. Ouahab *Inorg. Chem. Front.* **2017**, *4*, 604-617.

Entry for the Table of Contents

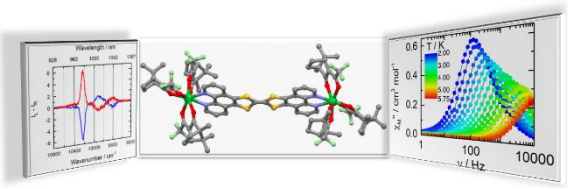

A redox-active chiral near-infrared circularly polarized luminescent field-induced single-molecule magnet of Yb^{III} at the solid-state was designed from the bridging of two $Yb(facam)_3$ units with the bis(1,10-phenantro[5,6b])tetrathiafulvalene triad.